SCIENCE CHINA
Technological Sciences

•Article•

December 2023 Vol.66 No.12: 3628–3638
https://doi.org/10.1007/s11431-022-2341-x

Transcranial direct current stimulation inhibits epileptic activity propagation in a large-scale brain network model

YU Ying[1], FAN YuBo[2], HAN Fang[3*], LUAN GuoMing[4] & WANG QingYun[5,6*]

[1] *School of Engineering Medicine, Beihang University, Beijing 100191, China;*
[2] *Beihang University, Beijing Advanced Innovation Center for Biomedical Engineering, School of Biological Science and Medical Engineering, Key Laboratory Biomechanics & Mechanobiology, Ministry of Education, Beijing 100191, China;*
[3] *College of Information Science and Technology, Donghua University, Shanghai 201620, China;*
[4] *Beijing Key Laboratory of Epilepsy, Sanbo Brain Hospital, Capital Medical University, Beijing 100069, China;*
[5] *Department of Dynamics and Control, Beihang University, Beijing 100191, China;*
[6] *Beijing Institute of Brain Disorders, Capital Medical University, Beijing 100069, China*

Received December 4, 2022; accepted February 8, 2023; published online November 20, 2023

Transcranial direct current stimulation (tDCS) is a noninvasive technique that uses constant, low-intensity direct current to regulate brain activities. Clinical studies have shown that cathode-tDCS (c-tDCS) is effective in reducing seizure frequency in patients with epilepsy. Due to the heterogeneity and patient specificity of seizures, patient-specific epilepsy networks are increasingly important in exploring the regulatory role of c-tDCS. In this study, we first set the left hippocampus, parahippocampus, and amygdala as the epileptogenic zone (EZ), and the left inferior temporal cortex and ventral temporal cortex as the initial propagation zone (PZ) to establish a large-scale epilepsy network model. Then we set tDCS cathode locations according to the maximum average energy of the simulated EEG signals and systematically study c-tDCS inhibitory effects on the propagation of epileptic activity. The results show that c-tDCS is effective in suppressing the propagation of epileptic activity. Further, to consider the patient specificity, we set specific EZ and PZ according to the clinical diagnosis of 6 patients and establish patient-specific epileptic networks. We find that c-tDCS can suppress the propagation of abnormal activity in most patient-specific epileptic networks. However, when the PZ is widely distributed in both hemispheres, the treatment effect of c-tDCS is not satisfactory. Hence, we propose dual-cathode tDCS. For epilepsy models with a wide distribution of PZ, it can inhibit the propagation of epileptiform activity in other nodes except EZ and PZ without increasing the tDCS current strength. Our results provide theoretical support for the treatment of epilepsy with tDCS.

epilepsy, large-scale brain network modeling, transcranial direct current stimulation, neural mass model

Citation: Yu Y, Fan Y B, Han F, et al. Transcranial direct current stimulation inhibits epileptic activity propagation in a large-scale brain network model. Sci China Tech Sci, 2023, 66: 3628–3638, https://doi.org/10.1007/s11431-022-2341-x

1 Introduction

The International League Against Epilepsy defines temporal lobe epilepsy (TLE) as a condition characterized by recurrent, unprovoked seizures originating from the medial or lateral temporal lobe [1]. Surgical intervention and pharmacological treatment are the common methods of seizure control [2,3]. However, these treatments are not always effective due to the obvious patient specificity of the epileptogenic zone (EZ) and the seizure propagation process [4]. Furthermore, the EZ is usually located in multiple brain regions and may involve eloquent areas that cannot be surgically resected [5,6]. Therefore, there is an urgent necessity to develop effective modulation methods to deal with patient specificity in seizures and minimize the impact on normal brain regions.

*Corresponding authors (email: yadia-han@dhu.edu.cn; nmqingyun@163.com)

Transcranial direct current stimulation (tDCS) is a non-invasive neuromodulation technique consisting mainly of a battery-powered current generator and two types of electrodes (cathode and anode) on the scalp [7–9]. The tDCS generates weak currents, which can cause changes in the membrane potential of cortical neurons. The modulation of tDCS has been tested in various neurological diseases, such as Parkinson's disease, epilepsy, Alzheimer's disease, depression, and chronic pain disorders [10–14]. It is generally believed that anodal stimulation enhances the excitability of the targeted cortical network, while cathodal stimulation acts mainly to inhibit cortical excitability. In particular, cathode-tDCS (c-tDCS) has been used in various types of epilepsy to reduce seizure area excitability [15,16]. In seizure control applications, the tDCS cathode is usually placed at the location of the channel with the most active EEG epileptogenic activity, and the anode is located in the contralateral area or in the shoulder [17–19]. Fregni et al. [18] conducted the first controlled clinical trial of tDCS for epilepsy and found that c-tDCS significantly reduced epileptiform discharges. In subsequent studies, tDCS has been successfully used for the treatment of several types of epilepsy [20–22]. Most of these tDCS strategies are conventional, with one anode and one cathode configuration, while the HD-tDCS (cathode-centered 4×1 or 5×1 configuration) has also been studied [23–25]. Notably, c-tDCS has been shown to be safe and effective in the control of epileptiform discharges in most trials [10,15,16].

Although tDCS can reduce seizure frequency, there is significant heterogeneity in stimulation parameters, electrode position, and electrode size during stimulation. In addition, the mechanism of tDCS treatment remains unclear. Dynamical modeling analysis and network science currently provide a toolset for studying the electrophysiological activity of the nervous system and the mechanisms and regulatory approaches of types of neurological disorders [26–30]. Computational models have been used to study the mechanisms triggered by tDCS [31,32], such as the common "λE model", where λ denotes the "effective" membrane space constant [33]. Based on this model, Kunze et al. [34] applied it to a large-scale brain network and explored the effect of tDCS on resting-state functional connectivity. In epilepsy modulation, a new computational model was recently developed by Denoyer et al. [35] that combined synaptic plasticity at the neuronal level to explain the acute and long-lasting effects of tDCS on epileptic activity. Since tDCS is placed on the surface of the scalp, it has effects on multiple brain regions. Therefore, in this work, we explore the regulatory effects of tDCS based on the epilepsy network established at large-scale brain networks. Similar to previous studies, the brain is viewed as a network of oscillators containing multiple interconnected nodes [36–38]. Each node represents a brain region. Seizure is characterized by abnormally active oscillatory behaviors in the network at the macroscopic level. The high-amplitude oscillatory activity commonly denotes seizure dynamics, and low-amplitude irregular dynamics are considered a non-seizure state [4,39,40]. The brain region responsible for the origin or early organization of epileptic activity is called the EZ, and the area that is first recruited during the evolution of the episode is considered the initial propagation zone (PZ) [39]. We set up EZ and PZ nodes in the network to establish the epileptic brain network model, based on which we explore the modulation effect of tDCS. Moreover, we set specific EZ and PZ with the clinical diagnosis of six patients with TLE to construct epileptic brain network models with patient specificity. Then we apply the tDCS with different cathodal targets to control the propagation of seizures. Finally, for epilepsy models with a wide distribution of PZ, we also propose a dual-cathode tDCS. It can suppress seizure propagation, keeping the current strength consistent with the one-cathode setting. We hope that this work provides some theoretical guidance for subsequent tDCS treatment of epilepsy.

2 Methods

2.1 Large-scale brain network model

A total of 74 brain regions, with 37 cerebral areas in each hemisphere, are considered [34]. This area parcellation is based on the mixture of diffusion spectral imaging data and the CoCoMac database [41]. It contains the common EZ and propagation area of TLE and can be used to study the spatiotemporal dynamics characteristics of TLE. The connection matrix w_{ij} contains four values, 0, 1, 2, and 3, representing absent, weak, moderate, and strong connections. In addition, we also consider the transmission delay between different regions based on the tract lengths matrix and propagation velocity. The abbreviations of brain regions can be found in Table S1.

Temporal dynamics of different regions are simulated using the Jansen-Rit model and assuming that all 74 regions (i.e., network nodes) have the same standard parameterization. The Jansen-Rit model contains excitatory pyramidal neuron populations, excitatory interneuron populations, and inhibitory interneuron populations (Figure 1) [42]. Each neural population is modeled by two blocks. The first is the postsynaptic potential (PSP) block, which is represented by an impulse response function:

$$h_E(t) = \begin{cases} Aat\mathrm{e}^{-at}, & t \geqslant 0, \\ 0, & t < 0, \end{cases} \tag{1}$$

$$h_I(t) = \begin{cases} Bbt\mathrm{e}^{-bt}, & t \geqslant 0, \\ 0, & t < 0, \end{cases} \tag{2}$$

where h_E and h_I represent excitatory and inhibitory

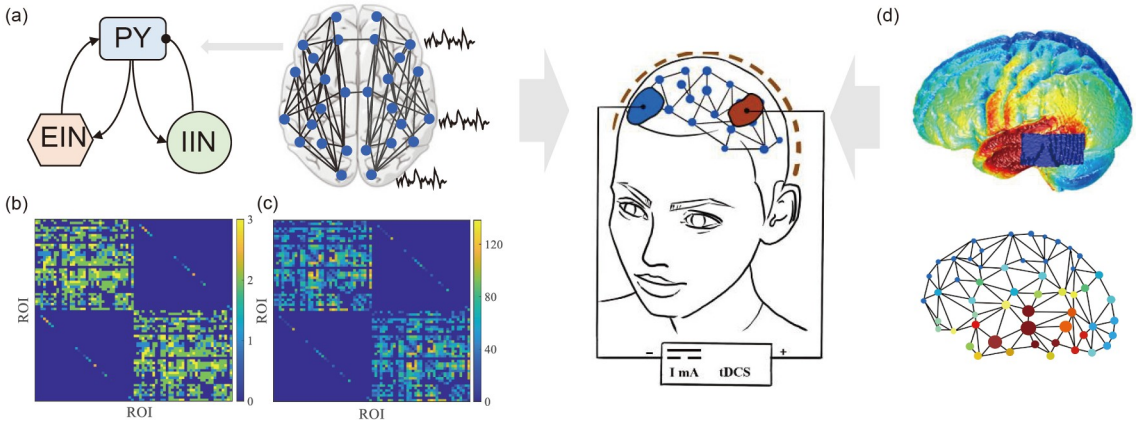

Figure 1 Whole-brain neural mass model and tDCS model. (a) Brain network model formed by 74 brain regions. The dynamic behavior of each region is described by the Jansen-Rit model. The Jansen-Rit model consists mainly of a pyramidal neural population (PY), a population of excitatory interneurons (EIN), and a population of inhibitory interneurons (IIN). (b) Heterogeneous connectivity matrix. (c) Tract lengths matrix. (d) Spatial voltage and electric field distributions obtained based on the cathode-anode position of tDCS. The area-specific distribution of tDCS-induced perturbations is determined, and a separate constant potential is added to each region during tDCS.

conditions, respectively. A and B are the maximum amplitudes of excitatory PSP and inhibitory PSP. a and b denote the inverse of the time constants in the excitatory and inhibitory feedback loops. The second block is to convert the average membrane potential of the neuronal population into the average pulse density, given by a sigmoid function of the form:

$$S(v) = 2e_0 / [1 + \mathrm{e}^{r(v_0 - v)}], \tag{3}$$

where e_0, r, and v_0 are the relevant parameters of the activation function. Different regions are interconnected to form a network based on the brain connectivity structure. The following set of differential equations describes the dynamic behavior of each area:

$$\begin{cases} \dot{x}_1^i = x_4^i, \\ \dot{x}_4^i = Aa\left[S(x_2^i - x_3^i + U_{\mathrm{tDCS}})\right] - 2ax_4^i - a^2 x_1^i, \\ \dot{x}_2^i = x_5^i, \\ \dot{x}_5^i = Aa\left[I + C_2 S(C_1 x_1^i) + K\sum_{j=1}^{N} w_{ij} S\left(x_2^j - x_3^j\right)\right] \\ \qquad -2ax_5^i - a^2 x_2^i, \\ \dot{x}_3^i = x_6^i, \\ \dot{x}_6^i = Bb[C_4 S(C_3 x_1^i)] - 2bx_6^i - b^2 x_3^i, \end{cases} \tag{4}$$

where x_1^i, x_2^i, and x_3^i are the outputs of the PSP blocks. $x_2^i - x_3^i$ is used as the output of the ith area. A, B, a, and b are consistent with eq. (1). N is the total number of network nodes. The connectivity constants C_1, C_2, C_3, and C_4 reflect the average number of synapses between the neural populations. K is a global coupling scale factor that can be interpreted as global axon density or effective chemicals acting on the efficacy of synaptic connection [34], and w_{ij} is the weighted connectivity. I is the excitatory current acting on the pyramidal subpopulation. U_{tDCS} is the equivalent voltage offset of tDCS. Furthermore, we add uncorrelated Gaussian noise to the pyramidal neural subpopulation [43]. The specific parameters of the model are shown in Table S2. In the follow-up study, the first 2 s of the time series are discarded, and the last 20 s are analyzed.

2.2 Simulated EEG data

We project the activity of 74 brain regions onto 62 EEG channels. Specifically, the activity of each area obtained from our calculations is propagated to a set of 62 EEG sensors through a propagation matrix. This propagation matrix is obtained by solving the boundary element method of the EEG forward problem and is available in the TVB dataset [44,45].

2.3 Combination of tDCS and large-scale brain network model

To calculate the spatial distribution of the effects of tDCS on each brain region, we simulate the electric field distribution of transcranial electrical stimulation using the ROAST open source software package [46]. We select the shape of the electrode "pad" and default the size of the electrode as [50 mm, 30 mm, 3 mm]. Homogeneous conductivity values of electrodes, skin, bone, air cavities, gray matter, and white are selected as default parameters in ROAST. For simplicity, we select the median value of voxel voltage ($Vol_{\mathrm{med}} = (V_{\max} + V_{\min})/2$) in the model voxel space and then set the voxel point with voltage below Vol_{med} as the cathode contribution (−1) and the voxel point above Vol_{med} as the anode contribution (+1). The area-specific distribution of the tDCS-induced perturbation γ at each voxel is the electric field magnitude multiplied by the cathode or anode contributions,

which effectively ensures the inhibitory effect of the cathode electrode on the brain area. γ can be expressed as

$$\gamma = ef(x,y,z) \cdot \text{sign}(Vol(x,y,z) - Vol_{\text{med}}), \quad (5)$$

where $ef(x, y, z)$ is the magnitude of the electric field at voxel coordinates (x,y,z), $Vol(x,y,z)$ is the voltage at voxel coordinates (x,y,z). Thus, γ incorporates both tDCS-induced electric field differences and cathodic and anodic contributions. To obtain the voltage offset induced by tDCS in the 74 brain regions, we determine the MNI coordinates corresponding to the 74 brain regions. We calculate the affine transformation matrix through the REST open source software package [47]. The voxel coordinates (x, y, z) corresponding to the MNI coordinates are obtained by inversion, and then the tDCS electric field intensity at the corresponding voxel coordinates is obtained. The specific voltage offset received by each brain region is

$$U_{\text{tDCS}} = \hat{u}_{\text{tDCS}} \cdot \gamma, \quad (6)$$

where $\hat{u}_{\text{tDCS}}$ is the global scale factor of tDCS intensity. So, the voltage offset U_{tDCS} applied to different brain regions is proportional to the electric field calculated by ROAST. Finally, based on the classical "λE" model, we simulate the effect of tDCS-induced polarization by adding a perturbation voltage to the mean membrane potential of pyramidal cells.

3 Results

3.1 Simulation of brain area activity under epileptic neural network

It is generally believed that seizures reflect abnormal synchronous behavior of the neuronal activities, resulting in a marked hyperexcitability activity at the regional level. In large-scale brain networks, we hypothesize the existence of epileptogenic and propagating regions associated with epilepsy initiation and quantify the ability of different regions to produce epileptic discharges using excitatory synaptic gains in the model. Figure 2(a) shows a diagram of the state transitions of an isolated node under different values of the excitatory synaptic gain A and external inputs I. Here we assume that each node transitions between two states, i.e., the resting state represented by dark blue color and the epileptic discharge states represented by the green and yellow colors. As the value of A increases, the external input required for the node to transition to the oscillation state decreases. Referring to the previous study [39], we set the excitatory synaptic gain A for the node of EZ, initial PZ, and other nodes to 3.6, 3.4, and 3.25, respectively. The generation of epileptic activity at different nodes in the network is driven by external inputs through the connectivity between nodes. To investigate the effects of connection weight on node activities, we fix I = 90 and present the state transitions of 74 regions under different connection weights (Figure 2(d)). The node transitions from the resting state to the discharging state as the global coupling factor K gradually increases with A = 3.25. When A is increased to 3.6, the brain nodes in the network are under epileptic activity even though the value of K is small. In the subsequent study, the epilepsy network model consists of the EZ, the initial PZ, and other nodes (Figure 2(e)). We fix I = 90 and K = 0.75 to better represent the characteristics of EZ and PZ nodes. The external input I = 90 ensures that the isolated node at A = 3.6 is in the oscillation state, while A = 3.25 and 3.4 are at resting states. K = 0.75 ensures that the initial PZ at A = 3.4 is more susceptible to epileptic activity in the network.

Brain areas such as the amygdala (AMYG), hippocampus (HC), and parahippocampal cortex (PHC) are often clinically resected, and models predict that these regions are the most likely epileptogenic sites [4]. Therefore, we first set the left limbic regions (left HC (lHC), left PHC (lPHC), and left AMYG (lAMYG)) as EZ and set the left inferior temporal cortex (lTCI) and left ventral temporal cortex (lTCV) as the initial PZ to construct the epileptic network. Further, we will also construct patient-specific epilepsy network models in conjunction with SEEG reports from epileptic patients. Figure 3(a) and (b) show the activity of each brain region under the normal and epileptic networks, respectively. In the normal network, each region shows a low-amplitude random discharge pattern, and regions in the epileptic network show distinct oscillatory behaviors. Here, regions 3, 10, 25, 32, and 35 represent the lAMYG, lHC, lPHC, lTCI, and lTCV, respectively. The EZ and PZ nodes show obvious oscillatory behavior first. The EZ nodes, such as lAMYG and lHC, discharge more regularly, and the oscillation frequency is about 3 Hz. Other secondary propagation areas gradually develop epileptic activities under the influence of network connections. With increasing time, most of the brain regions in the left hemisphere are recruited during seizure evolution, and a few regions of the right hemisphere, such as regions 41 and 60, are also influenced. Overall, this network model simulates the propagation of epileptogenic activity in the brain.

3.2 Simulation of c-tDCS effects on seizures

The selection of the tDCS cathode location is extremely important in seizure suppression. In previous clinical studies, the cathode is generally positioned over the area of strongest epileptiform activity, i.e., the area with the highest discharge amplitude or frequency, and the anode is located in the contralateral position or in the shoulder. To identify the cathode position, we first simulate the EEG signals of 62 channels reconstructed from the activity of 74 brain regions, as shown in Figure 4(a). Obvious epileptic activities can be

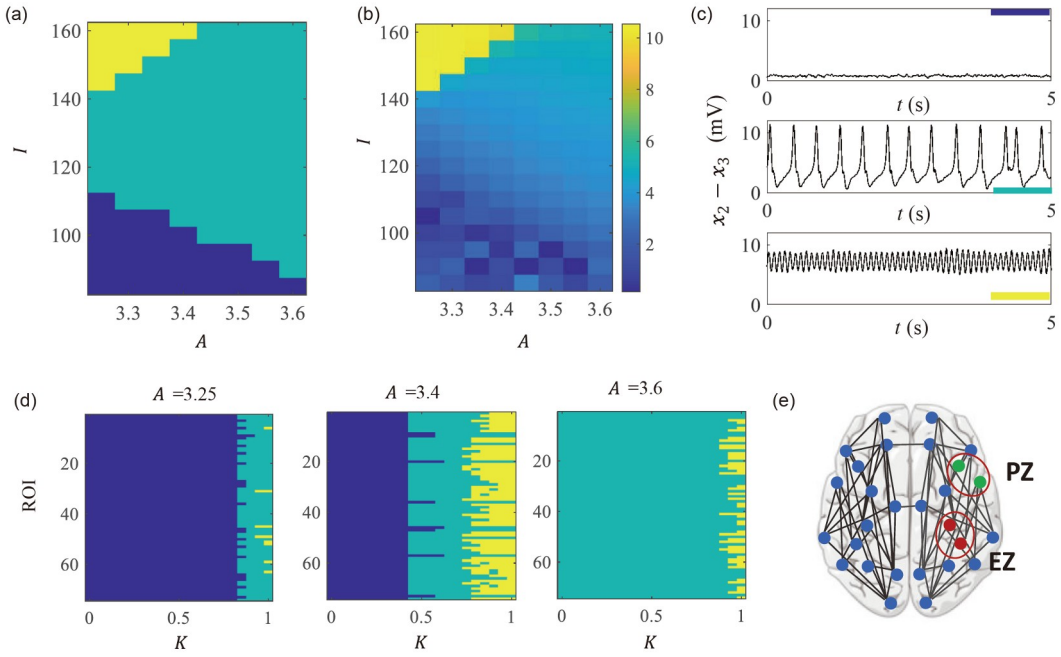

Figure 2 Dynamical transitions of isolated nodes and network nodes. (a) and (b) are the dynamic state analysis and frequency analysis of isolated nodes (i.e., $K = 0$) changing with excitatory synaptic gain A and external input I, respectively. Different colors in (a) represent different dynamic state areas, corresponding to the dynamic states given in (c). Dark blue indicates the resting state, and green and yellow indicate the oscillating state. As the applied current and synaptic gain increase, the node transitions from a resting state to an oscillatory state. (d) State transitions of 74 regions under different coupling scale factors with fixed A values. (e) Epilepsy network model consisting of the epileptogenic zone (EZ) ($A = 3.6$), the initial propagation zone (PZ) ($A = 3.4$), and other nodes ($A = 3.25$).

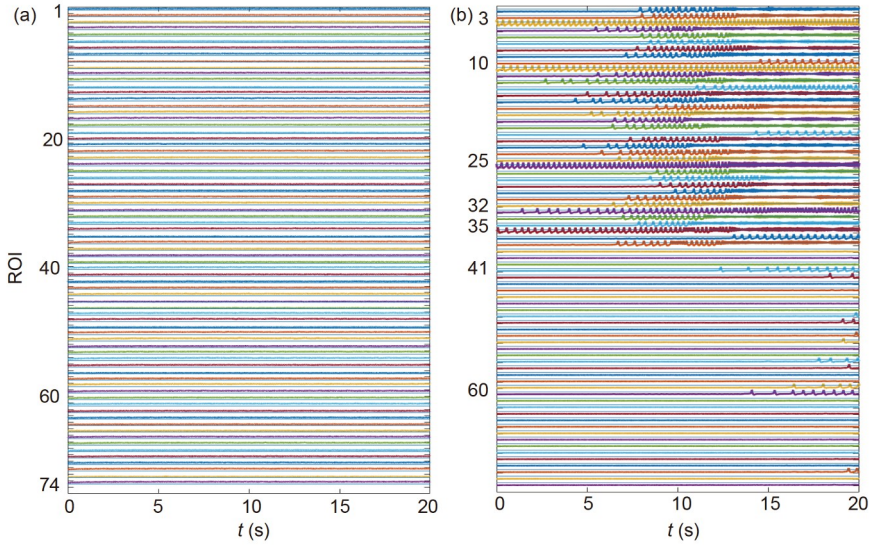

Figure 3 Time series plots of different brain regions under normal network and epileptic network models. (a) Different regions in a resting state under the normal network model. (b) Obvious oscillatory behaviors emerging in the epileptic network model. Regions 3, 10, 25, 32, and 35 represent the left AMYG (lAMYG), left HC (lHC), left PHC (lPHC), left inferior temporal cortex (lTCI), and left ventral temporal cortex (lTCV), respectively. The EZ is set to the lHC, lPHC, and lAMYG. The PZ is set to the lTCI and lTCV. In the seizure state, significant oscillatory behaviors are observed in the left hemisphere regions of the brain.

seen in the left EEG electrodes, such as F3, P3, P7, CP5, and PO3. Further, we separately calculate the energy of different EEG signals within 20 s and assume that the region with the highest energy is the area with stronger epileptic activities. The energy is defined as the integral of the power spectral density analysis curve of the EEG signal in the range of 0–50 Hz. The spectral analysis is performed with the Chronux neural signal analysis software package (www.chronux.org). As shown in Figure 4(b), we identify the cathode candidate position as CP5, corresponding to the

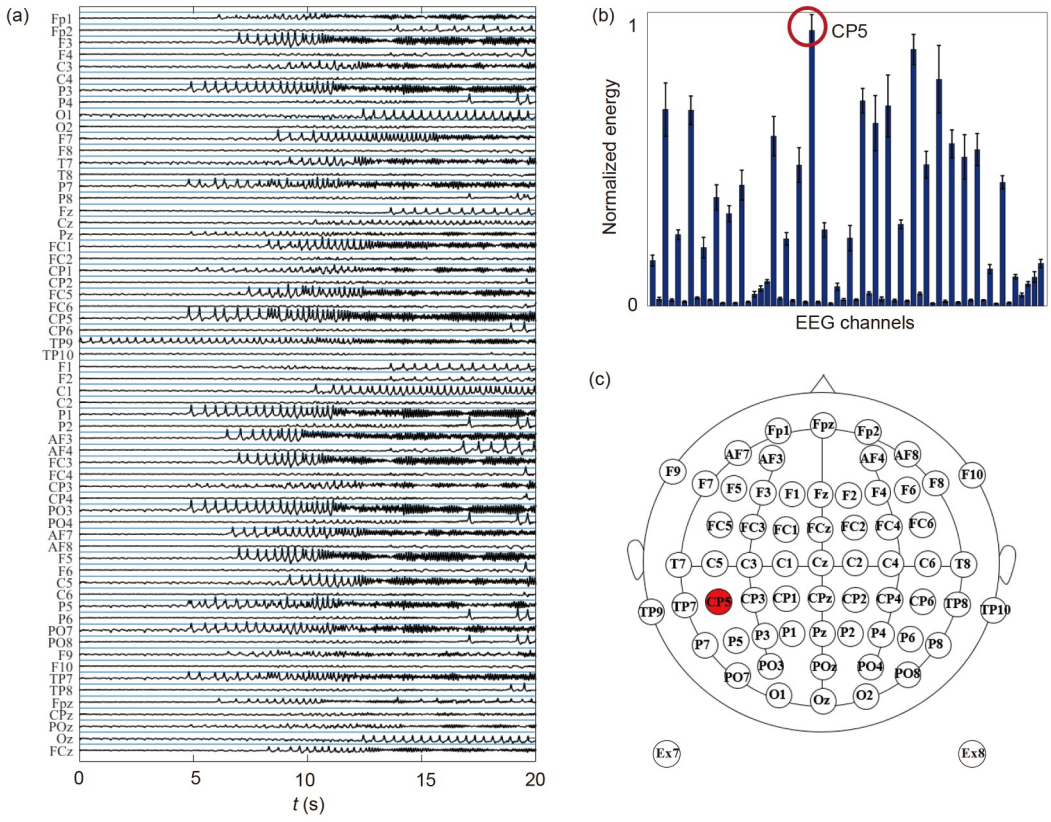

Figure 4 Simulated EEG signals with the corresponding energy analysis. (a) Simulated EEG signals obtained by projecting regional brain discharges onto 62 scalp EEG electrodes. Significant seizure discharge activities are observed at left EEG electrodes such as F3, P3, P7, CP5, and PO3. (b) Energy values of different channels derived and normalized based on the integration of the power spectral density analysis curves of the EEG signals in the range of 0–50 Hz. We count ten simulation results, and the standard deviations of the energy value fluctuations are represented by error bars. It is found that the CP5 channel corresponds to the maximum average energy. (c) Cathode and anode positions are shown in the EEG distribution map (cathode: CP5; anode: Ex8).

maximum average energy under ten simulation results. Based on the above electrode configuration, we further investigate the effect of c-tDCS on epilepsy suppression with the anode at Ex8 (additional electrode position of ROAST, non-epileptogenic zone) and the cathode set at CP5.

Figure 5(a) and (b) show the spatial distribution of voltage and electric field when 1 mA tDCS current intensity is applied (cathode: CP5; anode: Ex8). We obtain the electric field corresponding to 74 brain regions based on the description in Section 2, and γ for each brain region in the left hemisphere is shown in Figure 5(c). The area-specific perturbations in the left hemisphere are negative, thus ensuring that cathode stimulation reduces cortical excitability. The scaling factor $\hat{u}_{\mathrm{tDCS}}$ of the voltage offset reflects the strength of the c-tDCS to the global regions. Since tDCS is generally considered to be a weak stimulus, it does not cause neuronal firing. So, we assume that $\hat{u}_{\mathrm{tDCS}}$ varies from 0 to 1.5. With $\hat{u}_{\mathrm{tDCS}} = 0.5$, we find that c-tDCS fails to suppress seizures due to low intensity, but EZ and PZ take longer to affect other nodes compared with Figure 3(b) (Figure 5(d)). When $\hat{u}_{\mathrm{tDCS}}$ increases to 1.5, the c-tDCS effectively prevents the spread of epileptic activity, but regions 3, 10, 25, and 35 as epileptic EZ and initial PZ still present oscillatory activities (Figure 5(e)). Therefore, the effect of c-tDCS in a certain range is similar to blocking the transmission of abnormal signals and isolating the epileptogenic regions. Figure 5(f) shows the inhibition progress of epileptic activity in 74 brain regions as $\hat{u}_{\mathrm{tDCS}}$ increases from 0 to 1.5. The yellow area represents epileptiform activity, and the blue area represents the background activity. So, c-tDCS can suppress oscillatory activities in the right hemisphere regions with a rather small intensity. However, larger c-tDCS intensities are required to block the propagation of epileptic activity.

To investigate the effect of cathode position on the stimulation effect, we select CP5, P5, F5, C3, O1, P6, and F6 as the cathode locations and count the number of brain regions that still exhibit abnormal oscillatory activity under c-tDCS. As shown in Figure 5(g), tDCS with the cathode position at CP5 and P5 show significant effects on epilepsy inhibition. From EEG electrode locations, it can be found that the two electrodes are close to each other, and both are located in the left temporoparietal cluster. The F5, C5, and O1, which all belong to the left hemisphere, also inhibit the propagation of epilepsy to some extent. However, P6 and F6 as cathodic

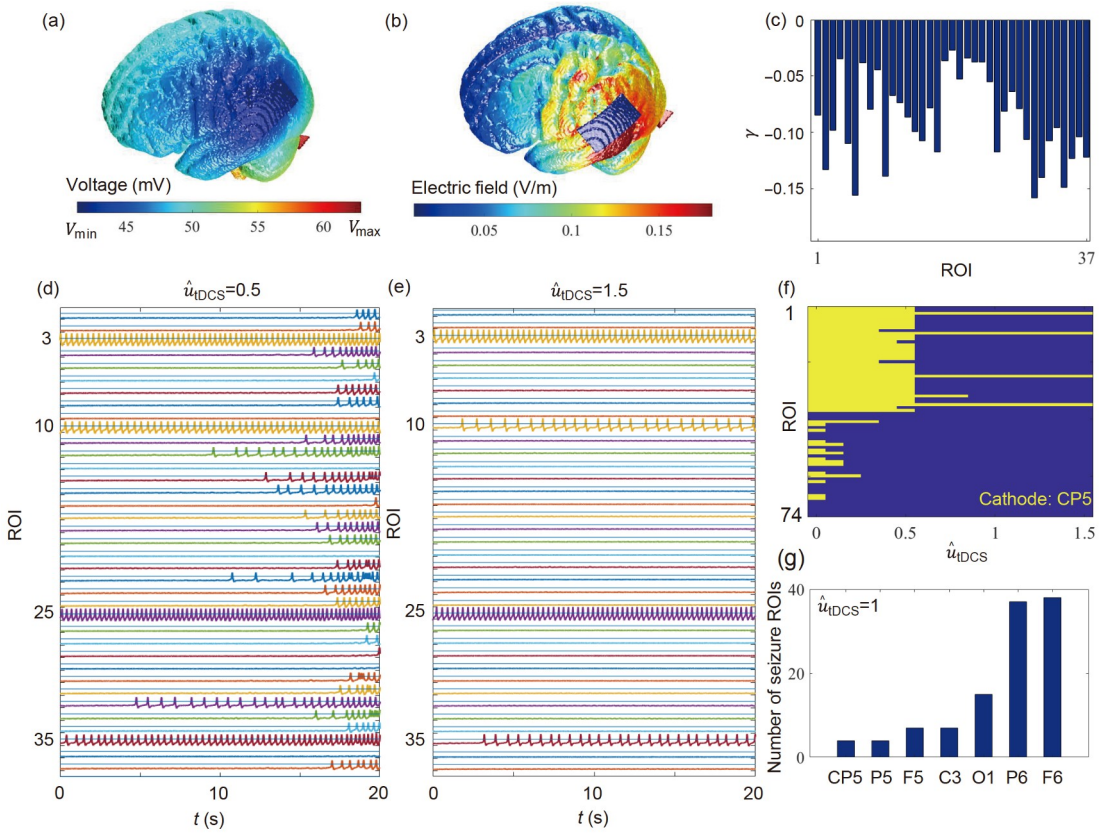

Figure 5 Effectiveness of c-tDCS in the control of epilepsy propagation. (a) and (b) are the spatial distributions of brain voltage and electric field at 1 mA tDCS current strength (cathode: CP5; anode: Ex8), respectively. (c) Area-specific distribution of the c-tDCS-induced perturbation in the left hemisphere regions. (d) and (e) are the effects of stimulation on the discharge behavior of different brain regions in the left hemisphere when $\hat{u}_{tDCS}$ = 0.5 and 1.5, respectively. (f) Inhibition progress of epileptic activity in 74 brain regions as $\hat{u}_{tDCS}$ increases from 0 to 1.5. The yellow area indicates the existence of oscillation behaviors, and the dark blue area indicates the restoration of the resting state. As $\hat{u}_{tDCS}$ increases, oscillatory behaviors are present only in regions 3, 10, 25, and 35, and tDCS effectively suppresses the propagation of epilepsy in other nodes. (g) Numbers of channels with oscillatory behavior under different c-tDCS. The inhibitory effect of c-tDCS on epilepsy is more significant when the cathode position is in the left EEG channels, but c-tDCS with the cathode position in the right EEG channel is not effective in suppressing seizures.

positions are ineffective in blocking the propagation of epileptic activities.

3.3 Simulation of c-tDCS effects on patient-specific epileptic networks

It is well known that there is significant patient specificity in epilepsy EZ and PZ. Due to this specificity, treatments such as surgery and medications are not always effective. Hence, we set specific EZ and PZ based on the clinical diagnosis of patients with TLE to establish patient-specific epilepsy networks. The specific EZ and PZ information of six patients in total is shown in Table 1. The EZ of these patients contains the hippocampus or amygdala, or both. The EZ of patient 5 also contains the central temporal cortex (TCC). The PZ of all patients involves the medial and lateral sides of the brain. The PZ of patients 1, 3, 4, 5, and 6 are located in one brain hemisphere, and the PZ of patient 2 involves both hemispheres. We simulate the brain regions' activities and corresponding EEG signals based on the epilepsy network model with specific EZ and PZ. The relatively high-energy channels in the simulated EEG signal are shown in Table 1, which are set as the cathode selection locations for the subsequent c-tDCS. For the epilepsy network model of patient 2, its PZ involves the right and left hippocampus, amygdala, TCC, and temporal pole (TOPOL). Therefore, there are high-energy EEG channels in both the left and right hemispheres. The EEG signal energy distribution for the different epilepsy networks is shown in Figure S1. The spatial distribution of c-tDCS voltage and electric field for different cathodes is shown in Figure S2.

Figure 6 shows the progression of c-tDCS inhibition of epileptic activity in 74 brain regions as $\hat{u}_{tDCS}$ increases. Similar to Figure 5(f), the yellow area represents the presence of epileptiform activity, and the blue area represents the background activity. We find that the distribution of EZ and initial PZ significantly impact the inhibition effect of c-tDCS. For the epilepsy network established by patients 1, 3, 4, 5, and 6, EZ and PZ only involve one hemisphere, and c-tDCS greatly reduces the spread of epileptic activities. The

Table 1 EZ, initial PZ, and cathode positions of six TLE patients

Patient	EZ	Initial PZ	Cathode position
1	lAMYG, lHC	lPHC, lCCR, lTCI, lTCS, lTCC	CP5
2	rAMYG	rHC, lHC, lAMYG, lTCC, rTCC, lTCPOL, rTCPOL	PO4, CP5
3	rAMYG	rHC, rPHC, rTCPOL, rTCC	PO4
4	rHC	rIA, rPCI, rCCP	CP6
5	lTCC, lHC	lAMYG, lTCI, lPHC	CP5
6	rAMYG, rHC	rCCP, rPCM, rPCI	CP6

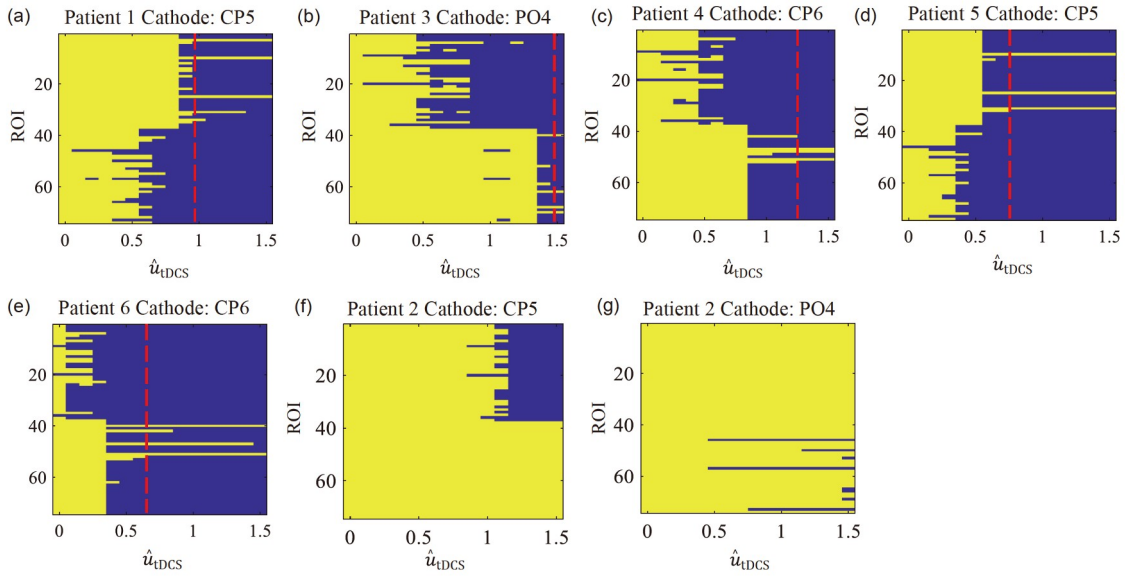

Figure 6 Effectiveness of c-tDCS in the control of different epileptic networks. (a)–(e) are the inhibition effects of c-tDCS on patients 1, 3, 4, 5, and 6 specific epileptic networks, respectively. The EZ and PZ in these patients involve only one hemisphere, and the spread of seizure activity gradually decreases with increasing $\hat{u}_{tDCS}$. The red line indicates the minimum intensity required for c-tDCS to suppress oscillation in all brain regions except the EZ and PZ nodes. (f) and (g) correspond to the inhibition effect of the patient-2-specific epileptic network. The PZ distribution in patient 2 involved both cerebral hemispheres, and c-tDCS treatment is not satisfactory.

red lines in Figure 6(a)–(e) represent the minimum intensity required for c-tDCS to inhibit oscillations in all brain regions except EZ and PZ nodes. The c-tDCS intensity required by different patients has obvious specificity, but the overall inhibition progress is similar. As the stimulation intensity increases, c-tDCS first suppresses epileptiform activities in brain regions contralateral to the epileptogenic zone. Larger intensities are required to suppress the oscillatory behavior of other nodes within the ipsilateral brain region. For patient 2, the c-tDCS effect is unsatisfactory. The PZ of patient 2 involves the hippocampus, amygdala, TCC, and TOPOL on the left and right sides of the brain. The PZ is too widely distributed compared with other patients. The c-tDCS failed to inhibit the propagation of epileptic activity in either cathode position CP5 or PO4. Therefore, we find that the stimulation intensity required by c-tDCS and the therapeutic effect depends on the distribution of PZ and EZ in patients.

To improve the stimulation range of c-tDCS, we propose a tDCS strategy with dual cathodal electrode pads. The two cathodes are placed on the two channels with high energy in the simulated EEG signals. As shown in Figure 7(a), we simulate the patient 2-specific epilepsy network and calculate the energy distribution of different EEG signals. The two cathode pads are placed on the two highest energy channels, CP5 and PO4, and the anode is placed on Ex8. The current intensity of 0.5 mA is applied to CP5 and PO4, thus ensuring the same total current strength as the single c-tDCS. Figure 7(b) presents the progression of the inhibition of the dual-cathode tDCS with the increase of $\hat{u}_{tDCS}$. Compared with Figure 6(f) and (g), the dual-cathode tDCS effectively inhibits the propagation of oscillation activities. We compare the electric field distribution generated by tDCS with CP5 as the cathode and tDCS with CP5 and PO4 as the cathode. The dual cathode increases the range of cathodic inhibition and effectively inhibits the propagation of the epileptic network with a wide distribution of PZ.

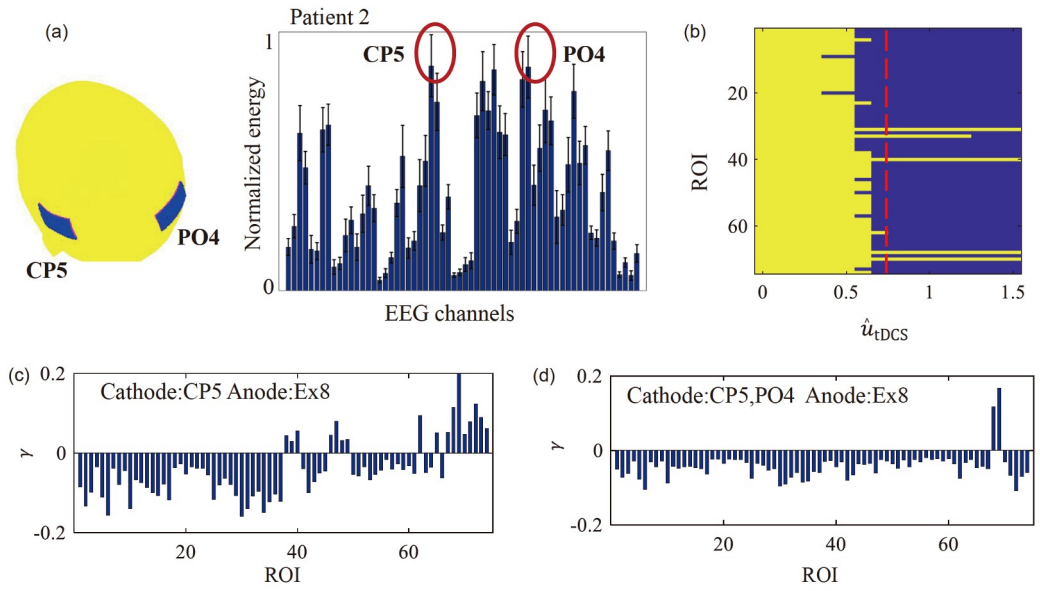

Figure 7 Effect of dual-cathode tDCS on the propagation of epilepsy. (a) Dual-cathode tDCS stimulation of the patient-2-specific epileptic network. Two cathodes are placed on the two high-energy channels of the simulated EEG signals (CP5 and PO4). (b) Effects of dual-cathode tDCS on the oscillatory behavior of 74 brain regions as $\hat{u}_{\text{tDCS}}$ increases. Compared with single-cathode stimulation, dual-cathode tDCS is effective in suppressing the propagation of epileptic activity. (c) and (d) are tDCS region-specific effect distributions, and dual-cathode tDCS improves the range of cathode inhibition for brain regions. Dual cathodes increase the range of cathodic inhibition.

4 Discussion and conclusion

Constructing computational models of epilepsy networks considering patient specificity is a hot issue of current studies. When using computational models to explore stimulation strategies, it is important to consider the specific EZ and PZ distributions. In this work, we view the brain as an oscillator with different nodes interconnected. Each node has two states, i.e., the background state and the seizure state. The oscillatory behavior, representing the seizure state, is thought to reflect an abnormal level of synchronization between neuronal activities. The low-amplitude random oscillation state represents the background state. To determine the cathode location for tDCS, we simulate the EEG signals and select the channels with relatively high-energy levels as the cathode candidate location. This is reasonable because seizures are always accompanied by abnormal excitation of neurons and a large increase in channel energy. Moreover, in clinical studies, the cathode is generally placed in the area with the strongest EEG epileptiform activity. We first set the lHC, lPHC, and lAMYG as EZ and the lTCI and lTCV as the initial PZ to construct the epileptic network. Next, the CP5 is selected as the cathode by EEG signal analysis. With increasing c-tDCS intensity, the propagation of epileptiform activity is inhibited, and the oscillatory activities in other regions except EZ and PZ are significantly reduced. To further explore the suppressive effect of c-tDCS on patient-specific epileptic networks, we select six TLE patients and determine the EZ and PZ based on their clinical diagnosis with SEEG reports. We find that the therapeutic effect of c-tDCS may be related to the distribution of EZ and initial PZ. When PZ is widely distributed in two hemispheres, the therapeutic effect of c-tDCS is not satisfactory. To improve the therapeutic range of c-tDCS, we propose dual-cathode tDCS, which increases the range of cathodal inhibition and effectively blocks the propagation of epileptic activity.

The following limitations still exist in this study. First, in terms of patient specificity, we only considered the differences in EZ and PZ among patients. At the same time, some studies use patient-specific structural connectome derived from data such as diffusion tensor imaging or diffusion-weighted MRI (dMRI) to establish models for the generation of neuroimaging signals, which seems more reasonable. Thus, a more reasonable individualized epilepsy network model considering the structural specificity should be constructed subsequently. Second, the established model only describes the transition between two states. It is well known that there are complex waveform oscillations in seizures, and we only considered the suppression of oscillatory behavior by c-tDCS. We did not further consider the transmigration between different waveforms. In addition, the current model does not reflect the different periods of seizure, such as interictal, preictal, and ictal. We only referred to the oscillatory state as the seizure state. We will further optimize the model in subsequent studies to explore the mechanism of the effect of tDCS on different periods of seizure. Third, for the patient-specific epilepsy network, we only considered 6 patients with TLE. Although it reflects the heterogeneity of EZ and PZ to some extent, the number of patients is relatively small. Our results are based on the epileptic networks of

these six patients. In the future, the study should be expanded to explore the modulatory effects of tDCS on more types of epileptic networks. Finally, the results only focus on the immediate effect of tDCS. Clinical studies have shown that tDCS can lead to long-term changes in the network through the effects of synaptic plasticity, and the mechanisms of long-term tDCS effects still need to be explored in future studies. In conclusion, by modeling the patient-specific epilepsy network, we explore the effect of the c-tDCS strategy for several common EZ and PZ distributions and propose a dual-cathode tDCS for suppressing the propagation of seizures, which may provide some theoretical guidance for future epilepsy treatment.

This work was supported by the National Natural Science Foundation of China (Grant Nos. 12202027, 11932003, 12272092, 11972115) and the China Postdoctoral Science Foundation (Grant No. 2021TQ0025).

Supporting Information

The supporting information is available online at tech.scichina.com and link.springer.com. The supporting materials are published as submitted, without typesetting or editing. The responsibility for scientific accuracy and content remains entirely with the authors.

1 Commission on Classification and Terminology of the International League Against Epilepsy. Proposal for Classification of Epilepsies and Epileptic Syndromes. Epilepsia, 1985, 26: 268–278
2 Perucca E, French J, Bialer M. Development of new antiepileptic drugs: Challenges, incentives, and recent advances. Lancet Neurol, 2007, 6: 793–804
3 Téllez-Zenteno J F, Dhar R, Wiebe S. Long-term seizure outcomes following epilepsy surgery: A systematic review and meta-analysis. Brain, 2005, 128: 1188–1198
4 Wang Y, Schroeder G M, Sinha N, et al. Personalised network modelling in epilepsy. arXiv: 1901.01024
5 Rolston J D. Surgical strategies for epilepsy in eloquent areas. J Epilepsy, 2016, 2: 1
6 Jehi L E, Silveira D C, Bingaman W, et al. Temporal lobe epilepsy surgery failures: Predictors of seizure recurrence, yield of reevaluation, and outcome following reoperation. JNS, 2010, 113: 1186–1194
7 Nitsche M A, Paulus W. Excitability changes induced in the human motor cortex by weak transcranial direct current stimulation. J Physiol, 2000, 527: 633–639
8 Nitsche M A, Cohen L G, Wassermann E M, et al. Transcranial direct current stimulation: State of the art 2008. Brain Stimul, 2008, 1: 206–223
9 Brunoni A R, Nitsche M A, Bolognini N, et al. Clinical research with transcranial direct current stimulation (tDCS): Challenges and future directions. Brain Stimul, 2012, 5: 175–195
10 Kaufmann E, Hordt M, Lauseker M, et al. Acute effects of spaced cathodal transcranial direct current stimulation in drug resistant focal epilepsies. Clin Neurophysiol, 2021, 132: 1444–1451
11 Boggio P S, Rigonatti S P, Ribeiro R B, et al. A randomized, double-blind clinical trial on the efficacy of cortical direct current stimulation for the treatment of major depression. Int J Neuropsychopharmacol, 2008, 11: 249–254
12 Broeder S, Nackaerts E, Heremans E, et al. Transcranial direct current stimulation in Parkinson's disease: Neurophysiological mechanisms and behavioral effects. Neurosci Biobehaval Rev, 2015, 57: 105–117
13 Fregni F, Boggio P S, Lima M C, et al. A sham-controlled, phase II trial of transcranial direct current stimulation for the treatment of central pain in traumatic spinal cord injury. Pain, 2006, 122: 197–209
14 Rajji T K. Transcranial magnetic and electrical stimulation in Alzheimer's disease and mild cognitive impairment: A review of randomized controlled trials. Clin Pharmacol Ther, 2019, 106: 776–780
15 Sudbrack-Oliveira P, Barbosa M Z, Thome-Souza S, et al. Transcranial direct current stimulation (tDCS) in the management of epilepsy: A systematic review. Seizure, 2021, 86: 85–95
16 San-juan D, Morales-Quezada L, Orozco Garduño A J, et al. Transcranial direct current stimulation in epilepsy. Brain Stimul, 2015, 8: 455–464
17 Tekturk P, Erdogan E T, Kurt A, et al. The effect of transcranial direct current stimulation on seizure frequency of patients with mesial temporal lobe epilepsy with hippocampal sclerosis. Clin Neurol Neurosurg, 2016, 149: 27–32
18 Fregni F, Thome-Souza S, Nitsche M A, et al. A controlled clinical trial of cathodal DC polarization in patients with refractory epilepsy. Epilepsia, 2006, 47: 335–342
19 Auvichayapat N, Rotenberg A, Gersner R, et al. Transcranial direct current stimulation for treatment of refractory childhood focal epilepsy. Brain Stimul, 2013, 6: 696–700
20 Varga E T, Terney D, Atkins M D, et al. Transcranial direct current stimulation in refractory continuous spikes and waves during slow sleep: A controlled study. Epilepsy Res, 2011, 97: 142–145
21 Yook S W, Park S H, Seo J H, et al. Suppression of seizure by cathodal transcranial direct current stimulation in an epileptic patient—A case report. Ann Rehabil Med, 2011, 35: 579
22 San-Juan D, Espinoza López D A, Vázquez Gregorio R, et al. Transcranial direct current stimulation in mesial temporal lobe epilepsy and hippocampal sclerosis. Brain Stimul, 2017, 10: 28–35
23 Meiron O, Gale R, Namestnic J, et al. High-definition transcranial direct current stimulation in early onset epileptic encephalopathy: A case study. Brain Injury, 2018, 32: 135–143
24 Meiron O, Gale R, Namestnic J, et al. Antiepileptic effects of a novel non-invasive neuromodulation treatment in a subject with early-onset epileptic encephalopathy: Case report with 20 sessions of HD-tDCS intervention. Front Neurosci, 2019, 13: 547
25 Rezakhani S, Amiri M, Weckhuysen S, et al. Therapeutic efficacy of seizure onset zone-targeting high-definition cathodal tDCS in patients with drug-resistant focal epilepsy. Clin Neurophysiol, 2022, 136: 219–227
26 Majhi S, Perc M, Ghosh D. Dynamics on higher-order networks: A review. J R Soc Interface, 2022, 19: 20220043
27 Parastesh F, Jafari S, Azarnoush H, et al. Chimeras. Phys Rep, 2021, 898: 1–114
28 Gosak M, Milojević M, Duh M, et al. Networks behind the morphology and structural design of living systems. Phys Life Rev, 2022, 41: 1–21
29 Ma J. Biophysical neurons, energy, and synapse controllability: A review. J Zhejiang Univ Sci A, 2022, 24: 109–129
30 Wu S F, Wang L B, Zhao Y W, et al. Chronic electrical stimulation induces functional network changes in cortical neuron cultures. Sci China Tech Sci, 2020, 63: 637–647
31 Lu H, Gallinaro J V, Rotter S. Network remodeling induced by transcranial brain stimulation: A computational model of tDCS-triggered cell assembly formation. Network Neurosci, 2019, 3: 924–943
32 Rahman A, Lafon B, Bikson M. Multilevel computational models for predicting the cellular effects of noninvasive brain stimulation. In: Progress in Brain Research. Elsevier, 2015. 25–40
33 Molaee-Ardekani B, Márquez-Ruiz J, Merlet I, et al. Effects of transcranial Direct Current Stimulation (tDCS) on cortical activity: A computational modeling study. Brain Stimul, 2013, 6: 25–39
34 Kunze T, Hunold A, Haueisen J, et al. Transcranial direct current stimulation changes resting state functional connectivity: A large-scale brain network modeling study. NeuroImage, 2016, 140: 174–187
35 Denoyer Y, Merlet I, Wendling F, et al. Modelling acute and lasting effects of tDCS on epileptic activity. J Comput Neurosci, 2020, 48:

161–176
36 Jirsa V K, Proix T, Perdikis D, et al. The Virtual Epileptic Patient: Individualized whole-brain models of epilepsy spread. Neuroimage, 2017, 145: 377–388
37 Liu Z L, Yu Y, Wang Q Y. Functional modular organization unfolded by chimera-like dynamics in a large-scale brain network model. Sci China Tech Sci, 2022, 65: 1435–1444
38 Coronel-Oliveros C, Cofré R, Orio P. Cholinergic neuromodulation of inhibitory interneurons facilitates functional integration in whole-brain models. PLoS Comput Biol, 2021, 17: e1008737
39 Yang C, Liu Z, Wang Q, et al. Epileptic seizures in a heterogeneous excitatory network with short-term plasticity. Cogn Neurodyn, 2021, 15: 43–51
40 Yang C, Luan G, Wang Q, et al. Localization of epileptogenic zone with the correction of pathological networks. Front Neurol, 2018, 9: 143
41 Kötter R. Online retrieval, processing, and visualization of primate connectivity data from the CoCoMac database. Neuroinformatics, 2004, 2: 127–144
42 Jansen B H, Rit V G. Electroencephalogram and visual evoked potential generation in a mathematical model of coupled cortical columns. Biol Cybern, 1995, 73: 357–366
43 Kulik S D, Douw L, van Dellen E, et al. Modeling of individual neurophysiological brain connectivity. Neuroscience, 2022
44 Sanz-Leon P, Knock S A, Spiegler A, et al. Mathematical framework for large-scale brain network modeling in The Virtual Brain. Neuroimage, 2015, 111: 385–430
45 Sanz Leon P, Knock S A, Woodman M M, et al. The Virtual Brain: A simulator of primate brain network dynamics. Front Neuroinform, 2013, 7: 10
46 Huang Y, Datta A, Bikson M, et al. Realistic volumetric-approach to simulate transcranial electric stimulation—ROAST—A fully automated open-source pipeline. J Neural Eng, 2019, 16: 056006
47 Pion-Tonachini L, Hsu S H, Chang C Y, et al. Online automatic artifact rejection using the real-time EEG source-mapping toolbox (REST). In: 2018 40th Annual International Conference of the IEEE Engineering in Medicine and Biology Society (EMBC). Honolulu: IEEE, 2018. 106–109